Microwave Assisted Flow Synthesis: Coupling of Electromagnetic and Hydrodynamic Phenomena

Narendra G. Patil, Faysal Benaskar, Jan Meuldijk, Lumbertus A. Hulshof, Volker Hessel, and Jaap C. Schouten
Laboratory of Chemical Reactor Engineering, Eindhoven University of Technology, P.O. Box 513, 5600 MB Eindhoven, The Netherlands

Erik D. C. Esveld
Food and Biobased Research, Wageningen University, P.O. Box 17, 6700 AA, Wageningen, The Netherlands

Evgeny V. Rebrov
School of Chemistry and Chemical Engineering, Queen's University Belfast, Stranmillis Road, Belfast, BT9 5AG, United Kingdom

DOI 10.1002/aic.14552
Published online July 18, 2014 in Wiley Online Library (wileyonlinelibrary.com)

This article describes the results of a modeling study performed to understand the microwave heating process in continuous-flow reactors. It demonstrates the influence of liquid velocity profiles on temperature and microwave energy dissipation in a microwave integrated milli reactor-heat exchanger. Horizontal cocurrent flow of a strong microwave absorbing reaction mixture (ethanol + acetic acid, molar ratio 5:1) and a microwave transparent coolant (toluene) was established in a Teflon supported quartz tube (i.d.: 3×10^{-3} m and o.d.: 4×10^{-3} m) and shell (i.d.: 7×10^{-3} m and o.d.: 9×10^{-3} m), respectively. Modeling showed that the temperature rise of the highly microwave absorbing reaction mixture was up to four times higher in the almost stagnant liquid at the reactor walls than in the bulk liquid. The coolant flow was ineffective in controlling the outlet reaction mixture temperature. However, at high flow rates it limits the overheating of the stagnant liquid film of the reaction mixture at the reactor walls. It was also found that the stagnant layer around a fiber optic temperature probe, when inserted from the direction of the flow, resulted in much higher temperatures than the bulk liquid. This was not the case when the probe was inserted from the opposite direction. The experimental validations of these modeling results proved that the temperature profiles depend more on the reaction mixture velocity profiles than on the microwave energy dissipation/electric field intensity. Thus, in flow synthesis, particularly where a focused microwave field is applied over a small tubular flow reactor, it is very important to understand the large (direct/indirect) influence of reactor internals on the microwave heating process. © 2014 American Institute of Chemical Engineers *AIChE J*, 60: 3824–3832, 2014

Keywords: microwave-assisted continuous-flow synthesis, continuous-flow reactors, heating efficiency, modeling of coupled electromagnetic and hydrodynamic phenomena

Introduction

Fast and volumetric heating by microwaves is attracting attention for application in continuous-flow synthesis of specialty chemicals.[1,2] Major efforts in developing continuous-flow reactors for microwave assisted organic synthesis[3–11] demonstrate an increase of the reaction rate and product yield as compared to conventional heating.[6,11] In addition, the presence of hot spots,[3–5] efficiency of microwave heating,[6,7,10] and design of flow reactors[8–10] has been discussed. Most of these articles reveal the enhancement of the reaction rate or yields due to volumetric or selective nature of microwave heating. The high energy intensity of the focused microwaves, however, hampers the efficiency and controllability of operation especially when a strong microwave absorbing component is present.[12,13] In such scenarios, use of a microwave transparent coolant avoids overheating of the reaction mixture and at the same time permits extension of usable reactor lengths.[12,13] However, the use of a focused microwave field even in small well-defined reactor geometries does not always provide the expected temperature profiles.[13] This is majorly due to a lack of position specific information with respect to the velocity profile of the liquid,

This article is dedicated to the remembrance of one of the coauthors, Prof. Dr. L.A. (Bert) Hulshof, who passed away recently. In his work, at DSM and at Eindhoven University of Technology, Professor Bert Hulshof made many original and creative contributions to the field of Fine Chemical Process Development. In his work, Bert very successfully and systematically combined complex organic chemistry, catalysis and process technology. His systematic approach paved the way for efficient industrial scale production of many complex organic products. Bert's work on the application of microwave technology in chemical synthesis is groundbreaking. In this field he was a true pioneer.

Correspondence concerning this article should be addressed to J.C. Schouten at J.C.Schouten@tue.nl.

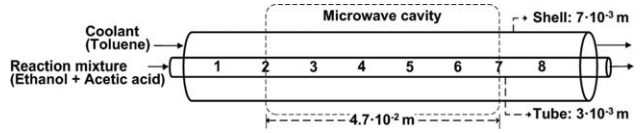

Figure 1. Schematic view and process details of the microwave integrated reactor-heat exchanger assembly used for experimental validation.

Numbers show the temperature measurement positions in the tube as well as in the shell.

that is, the reaction mixture. Additionally, the reliability of these predictions in microwave heating is limited when the spatial distribution of the volumetric heating source is not considered.[12]

Although experimentally demonstrated, the selective nature of microwave heating and the interaction of system components with the oscillating electric field of the microwaves is not explicitly understood in most of the cases.[14–18] Most reaction mixtures contain polar and nonpolar components, some interact with microwaves very strongly while others are completely microwave transparent. Additionally, many chemical reactors require some internals, for example, mixers, distributors, and measurement ports (i.e., temperature sensors), for various functions during operation. These internals in general influence the mixing/velocity profiles in the (batch/continuous) reactors and, consequently, can interfere in the microwave heating process. Therefore, at the early stage of process design, understanding of the system interactions (in a geometrical as well as in a fluid-dynamic sense) with microwaves and their influence on the microwave heating process are necessary to allow a robust process control and operation. Particularly in the case of flow reactors, the velocity profiles can strongly influence both processes, that is, heat transport and microwave absorption/interaction. Additionally, changes in the velocity profiles by reactor internals might add complexity to the microwave heating process. Especially, stagnant zones may have a considerable influence on heat transport and by that on the temperature profile. Therefore, it is of utmost importance to understand the spatial distribution of the intensity of microwave absorption and the corresponding local heating rate in the microwave heating process by detailed physical modeling.

The modeling efforts to understand the detailed mechanism of microwave assisted operation in combination with convective heat transport are largely applied in the food and drying industry.[19,20] In contrast, qualitative insight into the mechanisms behind microwave heating in reactive systems is rather limited.[21–24] Most of these efforts are used either to show the existence of a hot spot or to provide design guidelines for microwave applicators. Datta et al. have nicely demonstrated the possibility of combining the heat transfer and interactions of the oscillating electric field with the applied load, which they broadly referred as microwave combination heating.[25,26] These authors proposed an iterative procedure to reach the steady-state solution. In this iterative procedure, the temperature-change simulated by heat transfer, which consequently changed the dielectric properties of the load, was used to quantify interactions with the applied microwave field. In this study, similar approach is used to model the coupled phenomena in a continuous (milli) reactor-heat exchanger to see the influence of the liquid velocity profiles on the temperature and microwave energy absorption profiles (Figure 1).

Experimental Methods

Reactor assembly and flow regime

The continuous reactor-heat exchanger consists of a horizontal quartz tube (i.d.: 3×10^{-3} m and o.d.: 4×10^{-3} m) for the reaction mixture and a quartz shell (i.d.: 7×10^{-3} m and o.d.: 9×10^{-3} m), for the coolant (Figure 1). The reaction mixture is strongly microwave absorbing (ethanol + acetic acid, molar ratio 5:1), while the coolant (toluene) is microwave transparent. The purpose of the cocurrent coolant flow was to avoid overheating of the reaction mixture by the microwaves. Two Gilson high performance liquid chromatography (HPLC) pumps (flow range: $8.33 \times 10^{-9}-1.66 \times 10^{-6}$ m^3/s) are used to supply the reaction mixture and the coolant to the inner (reactor) tube and to the shell of the reactor-heat exchanger assembly, respectively. Measurements are performed, either with a low or with a high coolant velocity (Table 1), to study the influence of the cooling.

Microwave setup

The tubular milli reactor-heat exchanger assembly is perpendicularly fed through a vertical WR340 waveguide (Cavity, Figure 2). It is supported on each side by polytetrafluoroethylene (PTFE) cylinders in metal tubes (length 3×10^{-2} m and diameter 1.4×10^{-2} m). Thus, only the central part is exposed to the microwaves over a length of 4.7×10^{-2} m (Figure 1). Note that for the two reaction mixture flow rates studied (Table 1), the average heating time of the reaction mixture is only 0.18 and 0.44 s, respectively. The top of the cavity is shorted by an adjustable slider (short circuit, Figure 2) and the bottom of the cavity is coupled via a three stub tuner and an isolator with an antenna to a horizontal main waveguide. The main waveguide was connected to an adjustable generator which can provide up to 2 kW at the frequency of 2.45 GHz (Figure 2). Process control and data acquisition over the entire setup is performed via a custom made LABVIEW program. The dissipated power in the cavity could be determined from the recorded forward and reflected powers with an accuracy of approximately $\pm 10\%$.

Temperature measurements

The temperature inside the reactor tube and the surrounding shell is recorded at fixed positions (i.e., numbered positions in Figure 1) by microwave transparent fiber optic sensors (OpSense®, type OTG-A). The 1×10^{-3} m diameter of these probes was significant with respect to the only

Table 1. Operating Conditions for Modeling and Experimental Studies

	Reaction Mixture		Coolant		Microwave Power
Condition	Φ_R (10^{-7} m^3/s)	u_R (10^{-2} m/s)	Φ_C (10^{-9} m^3/s)	u_C (10^{-2} m/s)	P_{set} (W)
Slow coolant	16.67	26.5	8.33	0.03	~150
Fast coolant	6.66	10.6	1667	6.4	~60

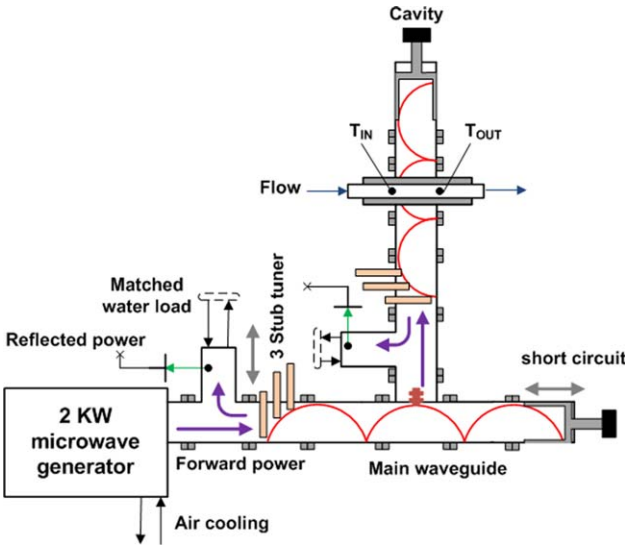

Figure 2. Schematic view of the microwave setup with an electric field pattern (red lines) in the setup.

Arrows signify flow of energy (purple), signals (green), liquids (blue), movement of stub tuner, and short circuit (gray). Actual load (reactor) opening diameter: 1.4 × 10^{-2} m. Design: TU Eindhoven. Manufacturer: Fricke und Mallah GmbH, Germany. [Color figure can be viewed in the online issue, which is available at wileyonlinelibrary.com.]

3×10^{-3} m inner diameter of the reactor tube. Two probes were initially inserted from either side of the assembly which stayed at least 3×10^{-2} m apart to maintain the empty volume in the microwave irradiation zone. Thus, temperatures were measured at Positions 1 to 4 with a probe from the left (i.e., inlet) and at Positions 5 to 7 with the probe from the right (i.e., outlet), see Figure 1. This, however, led to a serious misinterpretation of the temperature distribution inside the reactor tube. For more details, please see the discussion on the hot spot formation in our earlier publication.[12] The probe direction has a strong influence on the probe tip temperature. This effect will be discussed in detail in the Results and Discussion section.

Dielectric properties measurement

A high temperature dielectric probe kit (85070D, Agilent) and a network analyzer (NWA E5062A, Agilent) are used for the measurements of the dielectric constant (ε') and the dielectric loss (ε'') of the reaction mixture (ethanol + acetic acid, molar ratio 5:1) at a frequency of 2.45 GHz. The measurements of the batch sample at different temperatures are repeated and averaged over three runs (Figure 3). An oil bath was used to maintain the temperature at the desired value.

Modeling methods

The harmonic electromagnetic field, steady-state liquid flow and temperature in the setup are calculated with the finite element method in Comsol Multiphysics 4.2a (Figure 4). The laminar flowing fluid is heated by the microwaves and the heat is transported via convection to the outlet and via conduction to the coolant. The model is fully coupled as both the electromagnetic field pattern and the flow profile are determined by the temperature dependent permittivity, fluid density, and the viscosity. Temperature dependent material parameters are used as defined in the Comsol material library, where the reaction mixture (ethanol + acetic acid, molar ratio 5:1) is assumed to behave like pure ethanol. Only the complex permittivity of the reaction mixture was interpolated from the dielectric property measurements (Figure 3). The dielectric constant (ε') of toluene, quartz glass, and PFTE are 2.4, 4.2, and 2.0, respectively, and these materials have a negligible loss factor (ε'').

Electromagnetic field model

The modeled three-dimensional (3-D) geometry with the mesh is shown in Figure 4. Symmetry permitted modeling half of the complete geometry. The shape of the 2.45 GHz electromagnetic field depends on the metal enclosed geometry and the permittivity of the internal materials. The electric field should obey the Helmholtz equation which follows from the Maxwell equations in a source free domain (Eq. 1)

$$\nabla^2 E = \gamma^2 E \tag{1}$$

where E is the electric field intensity and the complex propagation constant γ in a medium is defined as

$$\gamma^2 = -\omega^2 \mu_0 \varepsilon_0 \left(\varepsilon' - j\varepsilon''\right) \tag{2}$$

where ω ($=2\pi f$) is the angular frequency, μ_0 is the magnetic permeability, ε_0 is the absolute permittivity of free space, and ε' and ε'' are the real (i.e., dielectric constant) and imaginary (i.e., dielectric loss) parts of the relative permittivity. The boundary condition at the perfect conducting metallic

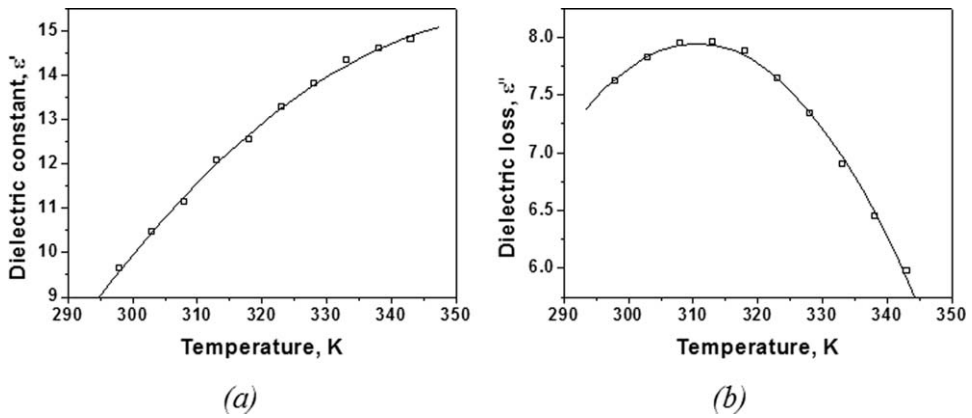

Figure 3. Dielectric constant, ε′ *(a)* and dielectric loss, ε″ *(b)* of the reaction mixture as a function of temperature.

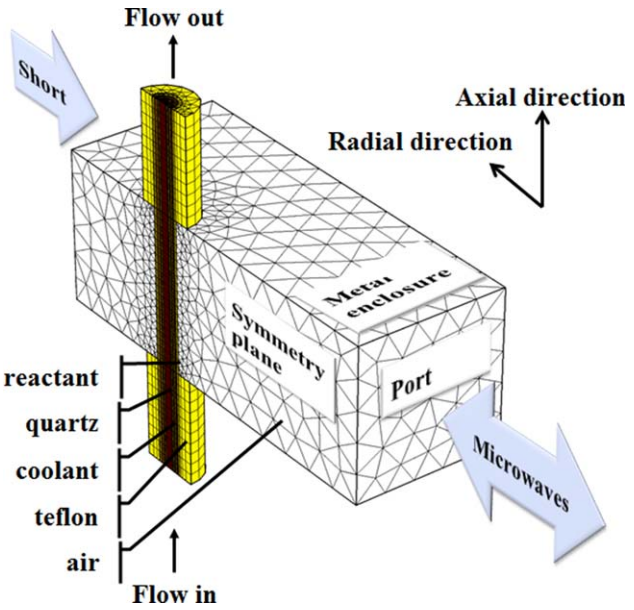

Figure 4. 3-D computational domain of the microwave cavity, showing individual components of the reactor assembly.

See Figure 1 for dimensions of the reactor assembly. [Color figure can be viewed in the online issue, which is available at wileyonlinelibrary.com.]

boundary is given by Eq. 3 and at the symmetry plane we have a perfect magnetic conductor (Eq. 4)

$$n \times E = 0 \tag{3}$$

$$n \times H = 0 \tag{4}$$

The field is excited at the open waveguide inlet port boundary (as shown in Figure 4) by a TE_{10} mode (Eq. 5)

$$E_z = E_0 \sin(\pi x/a) \tag{5}$$

where a is the waveguide width (i.e., 8.33×10^{-2} m) and x the coordinate over the broad side of the inlet with $x = 0$ at the symmetry plane. A two-dimensional (2-D) axial symmetric version of the same geometry is also modeled. The physics was the same except that in the latter case the rectangular waveguide is replaced by a cylindrical cavity of the same height and a diameter of 0.06 m. To excite the field in this case, we impose a uniform circular oscillating magnetic field H_ϕ at the outer cylindrical metallic wall.

Thermal model

The temperature is determined by a micro heat balance where convection and diffusion were augmented with the microwave source term (Eq. 6)

$$\rho C_p (u \cdot \nabla) T = -\nabla \cdot \left(-\hat{\lambda} \nabla T\right) + Q_{mw} P_{scale} \tag{6}$$

where u is the fluid velocity vector (which is zero in the solid) and $\hat{\lambda}$ is the effective thermal conductivity. The next section discusses the reasons behind using the effective thermal conductivity. The inlet and metallic boundaries are assumed to be at a fixed temperature (303 K) and the air is assumed to be perfectly isolating. Heating by viscous dissipation is ignored. The microwave energy density (Q_{mw}) is proportional to the square of the local root mean square value electric field (E_{rms}) and the imaginary part of the permittivity (ε''), see Eq. 7

$$Q_{mw} = \omega \varepsilon_0 \varepsilon'' E_{rms}^2 \tag{7}$$

Instead of tuning the driving boundary conditions to match the experimental conditions, the power density term Q_{mw} in Eq. 6 is multiplied by a scaling factor P_{scale} to equate the total heat source in the simulation with the experimental dissipated power P_{set} (Eq. 8)

$$P_{scale} = P_{set} / \int Q_{mw} dV_R \tag{8}$$

Flow model

The flow in the reaction mixture tube and coolant shell is determined by the Navier–Stokes momentum balance at the steady state

$$\rho (u \cdot \nabla) u = \nabla \cdot \left(-pI + \hat{\mu}\left(\nabla u + (\nabla u)^T\right) - \frac{2}{3}\hat{\mu}(\nabla \cdot u) I\right) + F \tag{9}$$

with the conservation of mass (constant density fluid)

$$\nabla \cdot (\rho u) = 0 \tag{10}$$

The fluid velocity (Table 1) and the pressure (ambient) are fixed at the two inlets, and no viscous stress is assumed at the outlets. The tubular walls have a no-slip condition. With the straight cylindrical geometry, this would result in simple parabolic Poiseuille profiles (except for a small deviation caused by the temperature dependent fluid properties). In the 3-D simulation, we included a vertical buoyancy force term (Eq. 11) related to the thermal expansion (density difference), since a mixed convection pattern could result from the horizontal flow

$$F_y = -g(\rho - \rho_{ref}) \tag{11}$$

In the 2-D simulation, this term was ignored. In the computationally lighter 2-D case, we have instead studied the effect of different fiber optic probe insertions. A disturbance to the flow profile, in the form of small recycles, is noted directly behind the probe tip. These cause an enhanced local mixing of momentum and heat. This cannot be resolved by a refinement of the grid and led to numerical instabilities. Therefore we used the so called low Reynolds κ/ε turbulence model in the 2-D case.[27] It is especially suited to preserve validity near the important stagnant boundary and does not need special wall functions. The intricate details of this turbulence model are outside the scope of this publication.[28,29] In short, it allows to estimate the extra momentum transport by the additional turbulent viscosity term in the effective viscosity (Eq. 12) which also enhances the effective thermal conductivity (Eq. 13, where the turbulent Prandtl number according to the Kays–Crawford model is about 1)

$$\hat{\mu} = \mu + \mu_T \tag{12}$$

$$\hat{\lambda} = \lambda + C_p \frac{\mu_T}{Pr_T} \tag{13}$$

The result is that the apparent diffusion of momentum and heat was 60 to 80% larger in the wake of the probe tip than in the pure laminar region.

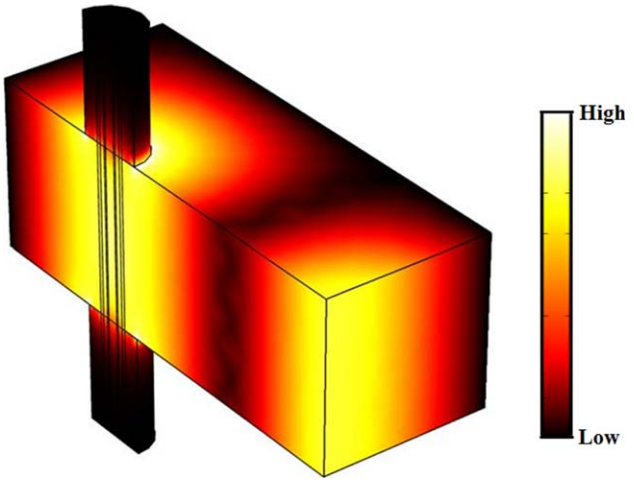

Figure 5. Electric field intensity (arbitrary unit) in and around the microwave integrated reactor-heat exchanger assembly.

See Figure 1 for dimensions of the reactor assembly. $\Phi_R = 6.66 \times 10^{-7}$ m^3/s, $\Phi_C = 1.66 \times 10^{-6}$ m^3/s, and $P_{set} = 60$ W. [Color figure can be viewed in the online issue, which is available at wileyonlinelibrary.com.]

Finite element solving procedure

Different strategies were used to solve the 3-D laminar flow with buoyancy and the 2-D flow with turbulent mixing behind the probe tip. In the 3-D case, the physics of the steady-state flow, the electromagnetic field and the heat transfer were implemented via the respective Comsol 4.2a application modes "single phase flow," "electromagnetic waves," and "heat transfer." These were sequentially solved to obtain a start solution. Then the fully coupled system was directly solved for 25 steps of increasing power toward P_{set} to converge towards the buoyancy driven recirculating flow. The mesh with in total only 18,793 elements (Figure 4) consisted of swept triangles with two elements at the boundary layer and at the nonslip interfaces, while a coarser free tetragonal mesh was used in the waveguide. With only about 30 K degree of freedom, the system is small enough to be solved within an hour on a PC. The flow and heat transfer in the 2-D model was implemented with the use of the application mode "nonisothermal flow." To resolve the extra κ and ε in turbulence parameters near the walls, an extra fine mesh (minimal and maximal edge length 0.05 and 0.4 mm) with nine boundary element layers was required in the flow

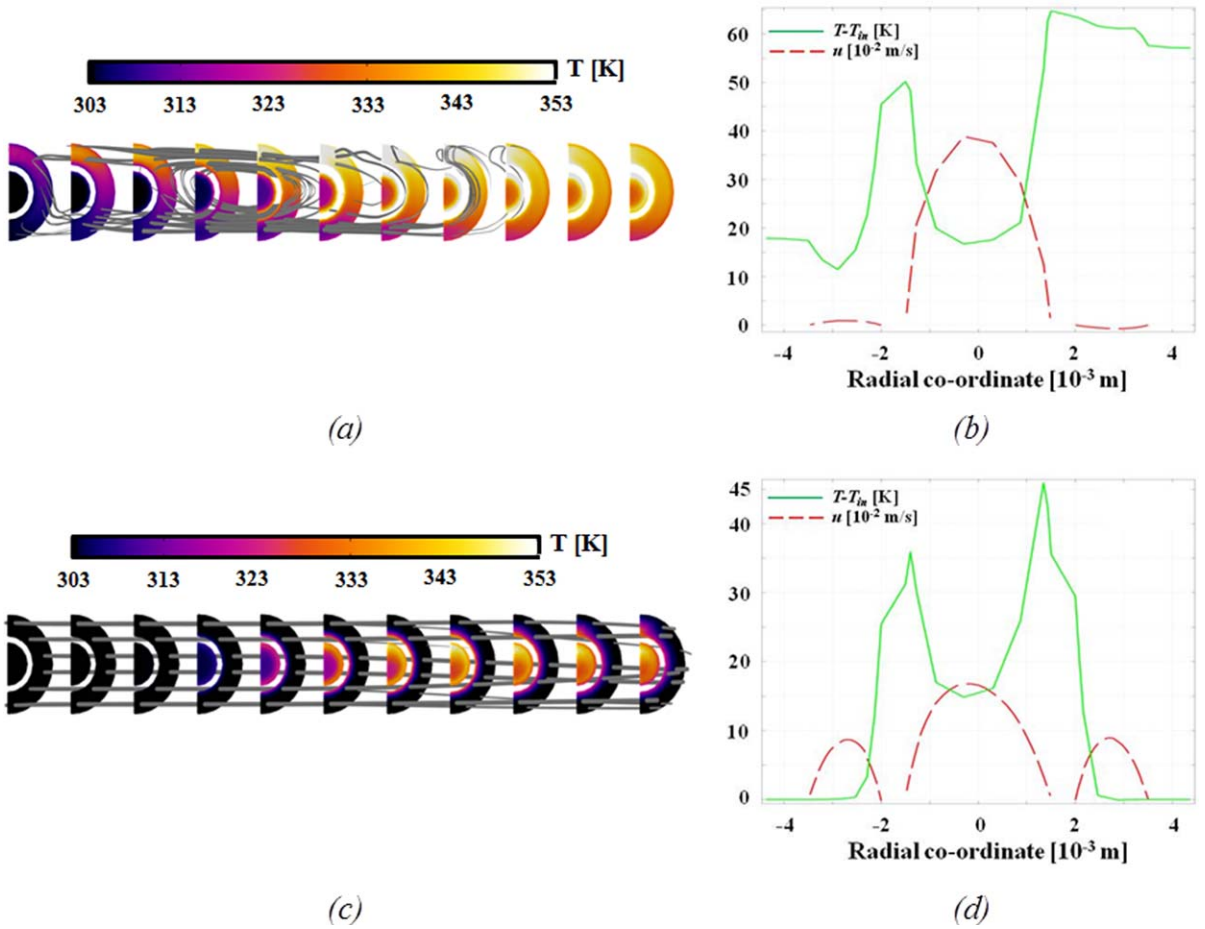

Figure 6. Effect of buoyancy in a horizontal arrangement of the microwave integrated reactor-heat exchanger assembly for slow coolant flow *(a, b)* and fast coolant flow *(c, d)* conditions.

***(a, c)*: contour plots. *(b, d)*: radial velocity and temperature profiles at axial coordinate of zero. Gray lines (with thickness indicating the strength) show the velocity profiles of the coolant in contour plots. The axially sectioned colored pattern shows the temperature of the reaction mixture and the coolant. *(a, b)*: slow coolant flow condition, $\Phi_R = 1.66 \times 10^{-6}$ m^3/s, $\Phi_C = 8.33 \times 10^{-9}$ m^3/s, and $P_{set} = 150$ W, *(c, d)*: fast coolant flow condition, $\Phi_R = 6.66 \times 10^{-7}$ m^3/s, $\Phi_C = 1.66 \times 10^{-6}$ m^3/s, and $P_{set} = 60$ W. [Color figure can be viewed in the online issue, which is available at wileyonlinelibrary.com.]**

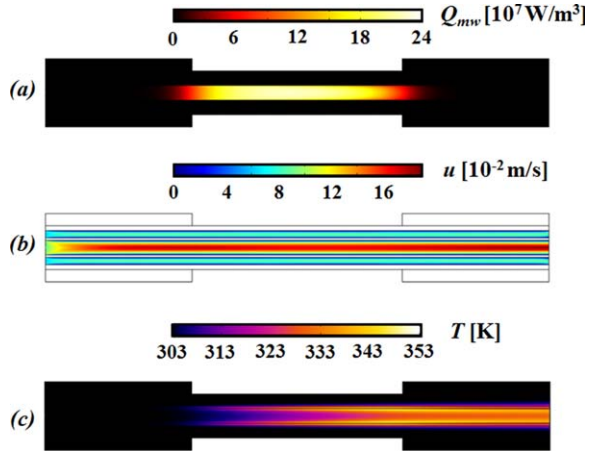

Figure 7. Profiles of microwave energy density *(a)*, velocity *(b)*, and temperature *(c)* obtained with the 2-D model.

See Figure 1 for dimensions of the reactor assembly. Fast coolant flow condition, $\Phi_R = 6.66 \times 10^{-7}$ m^3/s, $\Phi_C = 1.66 \times 10^{-6}$ m^3/s, and $P_{set} = 60$ W. [Color figure can be viewed in the online issue, which is available at wileyonlinelibrary.com.]

regime resulting in totally 17,797 elements. The whole system of 360 K degrees of freedom could be solved fully coupled for a single probe position within 15 min. In both case, a finer mesh did not show noticeable improvement in the solution. The standard convergence criteria of Comsol were used.

Results and Discussions

The calculated electric field intensity profile in the microwave cavity is shown in Figure 5. As the dielectric properties of the reaction mixture changed by a factor of two with temperature (Figure 3), it was intuitively expected that this would influence the electric field intensity along the reactor tube. However, this effect turned out to be of minor importance. Figure 5 shows that the position of the shorting plane in the waveguide can be chosen such that the electric field intensity of the standing wave is maximal at the reactor assembly. Furthermore, it can force the electric field to be almost cylindrically symmetric around the reactor axis.

Despite the fact that there was no difference in the electric field intensity between the feeding port and the shorting plane (see Figures 4 and 5), there was a nonsymmetric effect of the gravity due to the horizontal arrangement of the reactor-heat exchanger assembly. The buoyancy effect was very significant in the coolant section, particularly at the slow coolant flow condition in comparison to the fast coolant flow condition (Figure 6). In the slow coolant flow case, the temperature in the coolant section was up to 40 K higher at the top than at the bottom part of the assembly (Figure 6a). The upward force on the hot and thus less dense coolant fluid near the reactor tube induced a dominating fluid circulation pattern, as demonstrated in Figures 6a, b. Note that the circulating forward and backward coolant velocities are orders of magnitude larger than the net forward transport velocity of 0.3×10^{-3} m/s. Experimental validation of these modeling results was not possible due to a limited flexibility of the experimental setup. Nevertheless, it is important to note here that the horizontal arrangement of the reactor assembly, even at millimeter sized tubes, could show a significant gravitational influence on temperature and flow.

Figure 6 also shows that the temperature of the reaction mixture near the tubular wall was much higher than in the middle of the tube for both conditions. The radial distribution was studied in more detail with the 2-D model, which ignored the buoyancy effect. Figure 7 shows the distribution of the microwave energy density (Q_{mw}, Figure 7a), velocity (u, Figure 7b), and temperature (T, Figure 7c) with a reaction mixture flow rate of 6.66×10^{-7} m^3/s and a coolant flow rate of 1.66×10^{-6} m^3/s at an applied microwave power of 60 W. The dissipated microwave energy density was about 2.2×10^8 W/m^3 in the reaction mixture section (Figure 7a). The obtained velocity profile in the reaction mixture section was typical for laminar flow (Figure 7b). It was highest at the cylindrical symmetry (i.e., 18×10^{-2} m/s) and zero (i.e., a stagnant liquid film) at the reactor walls due to the no-slip boundary condition. The temperature of the reaction mixture increased linearly in the axial direction of the flow as a result of microwave absorption. It climbed from the inlet temperature of 303 to 328 K at the cylindrical symmetry (Figure 7c). However, at the inner reactor wall, the reaction mixture became much hotter (i.e., 353 K), thus reaching almost to the boiling point of ethanol. The coolant was microwave transparent and, therefore, the microwave energy density was zero in the coolant section (Figure 7a). Some convectively transferred heat from the reaction mixture was gained by the coolant, but the temperature in the bulk remained at the inlet temperature (303 K) due to the high coolant velocity (Figure 7c).

The coolant flow rate had a minor effect on the axial temperature profiles of the reaction mixture (Figures 8a, c), as almost identical axial temperature profiles of the reaction mixture were obtained for coolant flow rates of 8.33×10^{-9} and 1.66×10^{-6} m^3/s, respectively. Figures 8b, d show the radial profiles of velocity (u, red lines), temperature rise ($T-T_{in}$, green lines), and microwave energy density (Q_{mw}, blue lines) at the cylindrical symmetry for slow and fast coolant flow conditions. As mentioned earlier, in both cases, velocities of the reaction mixture and coolant had a near parabolic velocity profile (Figures 8b, d), except the coolant velocity was almost zero (Figure 8b) at the slow coolant flow condition. The temperature rise of the reaction mixture and the coolant ($T-T_{in} \approx 50$ K) was in this case highest near the reactor wall (Figure 8b). This is due to fact that the microwave heated stagnant reaction mixture film near the tube wall is not renewed. The microwave power density near the wall is actually less than in the middle, due to the decreasing dielectric loss with increasing temperature, but this has only a minor compensating effect. These observations suggest that the temperature depends more on the liquid velocity profile than on the microwave power density distribution, especially in systems where the focused microwave field is applied over tubular reactors with small diameters (i.e., in the millimeter range).

The temperature rise near the reactor wall resulted in a drop of the microwave energy density from 5.5×10^8 W/m^3 at the center of the reactor to 3×10^8 W/m^3 at the inner reactor wall (Figure 8b). This was due to the drop in the dielectric loss factor (ε'') at higher temperature (see Figure 3 and Eq. 7). However, with a high coolant flow rate, and a more effective convective cooling of the inner reactor wall, it shows a much smaller drop of the microwave energy

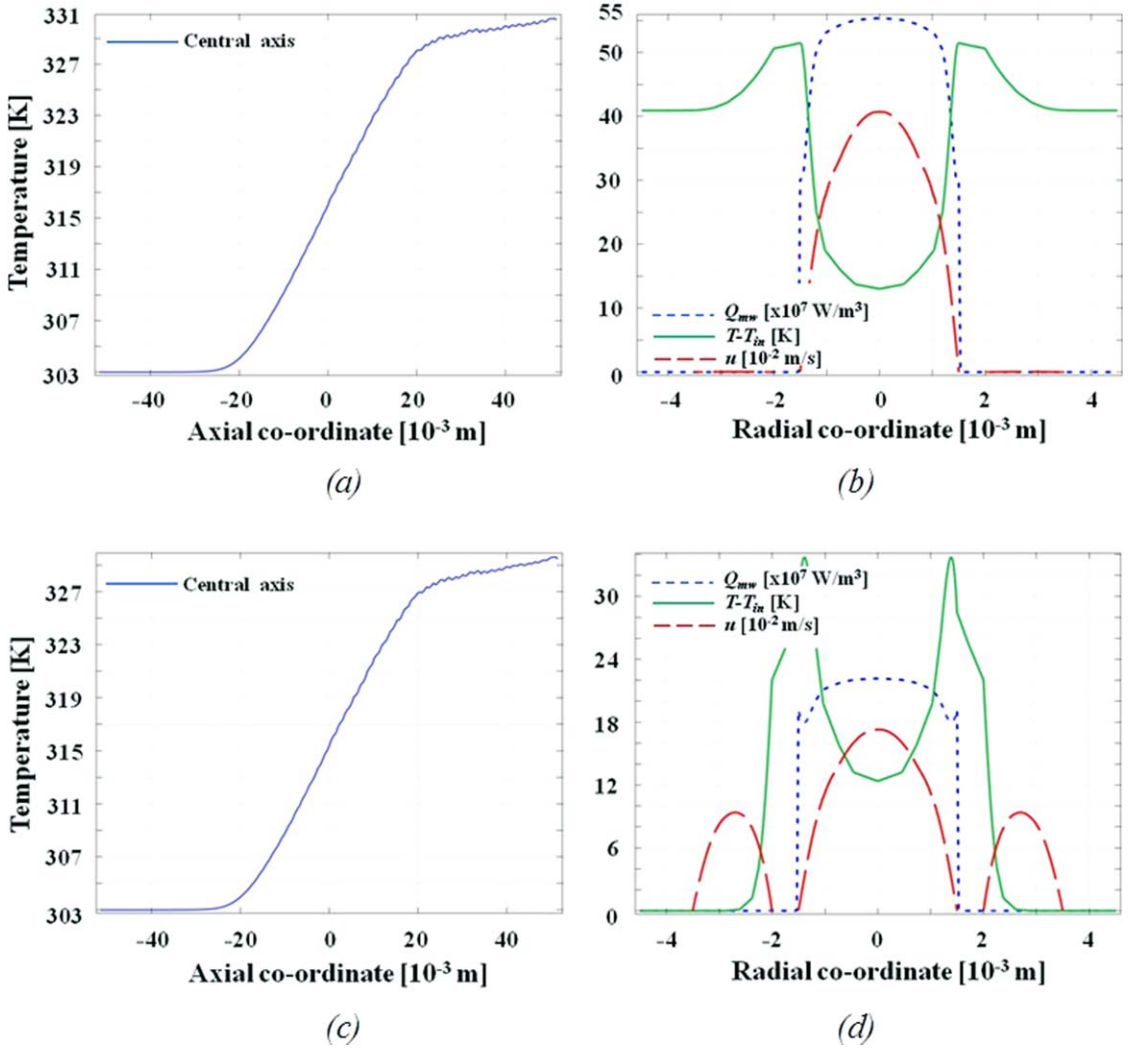

Figure 8. Axial temperature profiles *(a, c)* at cylindrical symmetry, and microwave energy density (Q_{mw}, W/m^3), temperature rise ($T–T_{in}$, K), and velocity (u, m/s) profiles *(b, d)* as a function of radial coordinate.

(a, b): **slow coolant flow condition, $\Phi_R = 1.66 \times 10^{-6}$ m^3/s, $\Phi_C = 8.33 \times 10^{-9}$ m^3/s, and $P_{set} = 150$ W,** *(c, d):* **fast coolant flow condition, $\Phi_R = 6.66 \times 10^{-7}$ m^3/s, $\Phi_C = 1.66 \times 10^{-6}$ m^3/s, and $P_{set} = 60$ W. [Color figure can be viewed in the online issue, which is available at wileyonlinelibrary.com.]**

density near the wall, and even a slight increase (Figure 8d). As a consequence, the coolant having only a minor influence on the reaction mixture outlet temperature (Figures 8a, c), allowed control over the microwave energy dissipation at the inner reactor wall (Figures 8b, d). This additional control provided by the coolant is definitely an interesting feature, for wall coated reactors where the reaction occurs at the catalyst film on the inner wall of the reactor.

The interpretation of the model results imply that any static internals in a microwave flow reactor, such as baffles or packed particles, will disturb the temperature distribution by disturbing the flow pattern. This was verified by inserting a microwave transparent fiber optic probe (commonly used for temperature measurement) in the geometry. Two separate cases were studied with the 2-D model, that is, insertion of the probe from the outlet (Figure 9a) and insertion of the probe from the inlet (Figure 9b).

The laminar flow of the reaction mixture rearranged itself around the probe which has a stagnant liquid film (no-slip condition). Just as observed earlier near the reactor wall, the liquid in the stagnant film surrounding the inserted probe

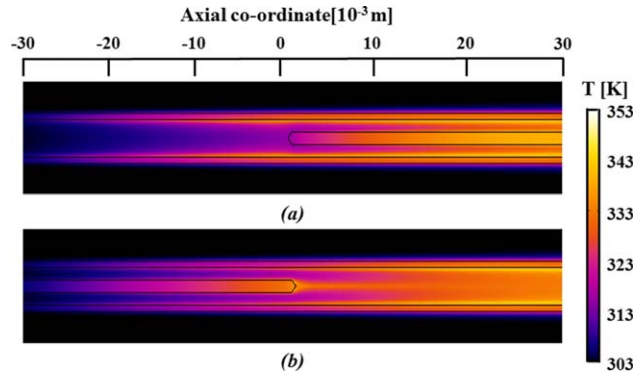

Figure 9. Influence of the direction of the probe insertion on the temperature profiles obtained by modeling, *(a)* probe inserted from the outlet and *(b)* probe inserted from the inlet.

See Figure 1 for dimensions of the reactor assembly. Fast coolant flow condition, $\Phi_R = 6.66 \times 10^{-7}$ m^3/s, $\Phi_C = 1.66 \times 10^{-6}$ m^3/s, and $P_{set} = 60$ W. [Color figure can be viewed in the online issue, which is available at wileyonlinelibrary.com.]

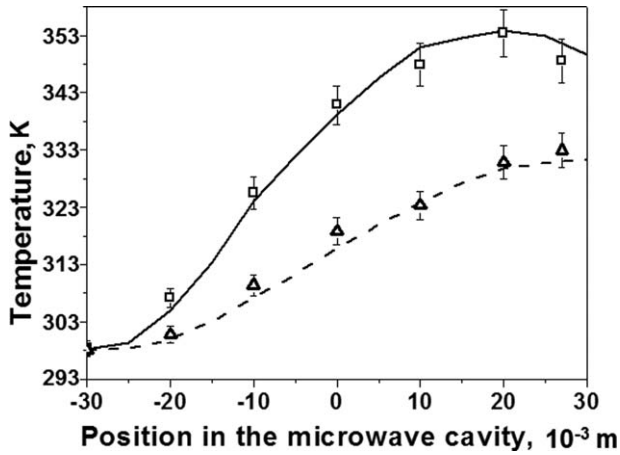

Figure 10. Influence of the direction of the probe insertion on the temperature profiles obtained by modeling (lines) and experiments (data points).

Solid line and squares: probe inserted from inlet, dotted line and triangles: probe inserted from outlet. Experimental as well as modeling condition: fast coolant flow, $\Phi_R = 6.66 \times 10^{-7}$ m^3/s, $\Phi_C = 1.66 \times 10^{-6}$ m^3/s, and $P_{set} = 60$ W.

also reached a higher temperature than the bulk liquid. Thus, the temperature measured by the probe is directly ruled by the temperature of the stagnant liquid film (Figure 9). This effect is seen to be building up from the cool inlet side to the hot outlet side. Now for the probe inserted from the outlet (Figure 9a), the stagnant film is just starting at the probe tip and it, therefore, shows the bulk temperature. Further downstream, the probe gets hotter, but that is not measured by the tip. Conversely, for the probe inserted from the inlet, the overheating of the stagnant liquid film is building up toward the probe tip and thus it shows a higher steady-state temperature (Figure 9b). In this case, it can be noticed that the hot zone continues for about 2×10^{-2} m directly after the probe tip (Figure 9b), because it takes some distance before the liquid at the center is accelerated to the bulk velocity and the excess heat is diffused away. These model observations for both cases, that is, insertion of the probe from the outlet and the inlet, were then validated by experiments (Figure 10).

Figure 10 shows the experimentally observed and calculated axial temperatures at different probe positions. The results in Figure 10 demonstrate that the model calculations were in excellent agreement with the experimental observations. The agreement of the theoretically calculated results with the observed experimental results confirms that the disturbances to the flow profile caused by the inserted probe (or reactor internals) have a considerable influence on the temperature distribution. Therefore, it is important to understand the direct (e.g., microwave absorption) or the indirect (e.g., disturbance to the velocity profile) influence of the reactor internals on the microwave heating process, in the case of processes where the selectivity is temperature dependent. Additionally, this approach of modeling can also be used in finding the reasons for reported hot spots in many of the microwave assisted flow synthesis studies. Although this modeling study is focused on volumetric liquid heating by the microwaves, for a better understanding it can also be expanded to processes where microwaves are used for selective heating of catalytically active metal films on the reactor walls.

Conclusions

A modeling study was conducted for milli-sized flow reactors to understand the influence of the velocity profiles on the microwave heating process. Almost stagnant zones in the microwave absorbing fluid influenced the temperature distribution in a microwave integrated flow reactor-heat exchanger. The temperature increase of the highly microwave absorbing reaction mixture was 2–4 times higher in the almost stagnant regions in the vicinity of the reactor walls compared to the bulk liquid. A buoyancy influence (as a result of gravitational forces) was clearly visible for a horizontal arrangement of a reactor-heat exchanger assembly at millimeter sizes, that is, a fluid circulation was observed due to density difference. The coolant flow was found to be ineffective in controlling the outlet reaction mixture temperature. However, the coolant at high flow rates limited the overheating and, consequently, improved the microwave energy dissipation at the inner reactor wall. Additionally, the disturbances to the velocity profile by reactor internals and their influence on the microwave heating process were investigated. The stagnant layer formation caused by insertion of a fiber optic probe from the inlet (i.e., from the direction of the flow) resulted in higher temperatures. The model predictions were experimentally validated and, therefore, demonstrated that the temperature profile depends more on the reaction mixture velocity profile than the electric field intensity, especially in systems where the focused microwave field is applied over a small tubular reactor. This study also shows that fully coupled simulation of microwave field and nonisothermal flow is feasible and required to understand the thermal performance of microwave heated flow reactors.

Acknowledgments

Authors would like to acknowledge Food and Biobased Research (Wageningen University, The Netherlands) for conducting the modelling and providing the dielectric property measurement equipment. They would also like to acknowledge DSM Research, Friesland-Campina, IMM, LioniX, Milestone s.r.l. and the Dutch Technology Foundation STW (project MEMFiCS GSPT-07974) for financial support.

Notation

a = waveguide width, 8.33×10^{-2}m
C_P = heat capacity, J/kg·K
E = electric field, V/m
E_0 = driving electric field amplitude, V/m
E_z = electric field at port parallel to tube, V/m
F = volume Force, N/m^3
F_y = buoyancy force in vertical direction, N/m^3
f = microwave frequency, 2.45×10^9 Hz
g = acceleration due to gravity, 9.80 m/s^2
H = magnetic field, A/m
I = identity matrix
n = normal direction
P_{set} = set microwave power, W
Pr_T = turbulent Prandtl number
p = pressure, Pa
Q_{mw} = microwave energy density, W/m^3
T = temperature, K

u = velocity, m/s
V_R = reactor volume, m^3

Greek letters

ε_0 = permittivity of free space, 8.854×10^{-12} F/m
ε' = dielectric constant
ε'' = dielectric loss
γ = complex propagation constant, 1/m
$\hat{\lambda}$ = effective thermal conductivity, W/m K
μ_0 = permeability of free space, $4\pi \times 10^{-7}$ H/m
$\hat{\mu}$ = effective dynamic viscosity, Pa s
μ_T = turbulent dynamic viscosity, Pa s
Φ_R = Reaction mixture flow rate, m^3/s
Φ_C = coolant flow rate, m^3/s
ρ = instantaneous Density, kg/m^3
ρ_{ref} = density at reference temperature, kg/m^3
ω = angular velocity ($2\pi f$), rad/s

Literature Cited

1. Roberts AB, Strauss RC. Towards rapid, 'green' predictable microwave-assisted synthesis. *Acc Chem Res*. 2005;38:653–661.
2. Shore G, Morin S, Organ MG. Catalysis in capillaries by Pd thin films using microwave-assisted continuous-flow organic synthesis (MACOS). *Angew Chem*. 2006;45:2761–2766.
3. Chemat F, Esveld E, Poux M, Di-Martino LJ. The role of selective heating in the microwave activation of heterogeneous catalysis reactions using a continuous microwave reactor. *J Microwave Power Electromagn Energy*. 1998;33:88–94.
4. Baxendale IR, Griffiths-Jones MC, Ley VS, Tranmer KG. Microwave-assisted Suzuki coupling reactions with an encapsulated palladium catalyst for batch and continuous-flow transformations. *Chem Eur J*. 2006;12:4407–4416.
5. Cecilia R, Kunz U, Turek T. Possibilities of process intensification using microwaves applied to catalytic microreactors. *Chem Eng Process*. 2007;46:870–881.
6. Esveld E, Chemat F, Haveren JV. Pilot scale continuous microwave dry-media reactor—part 1: design and modeling. *Chem Eng Technol*. 2000;23:279–283.
7. Esveld E, Chemat F, Haveren JV. Pilot scale continuous microwave dry-media reactor—part II: application to waxy ester production. *Chem Eng Technol*. 2000;23:429–435.
8. Plazl I, Pipus G, Koloini T. Microwave heating of the continuous flow catalytic reactor in a nonuniform electric field. *AIChE J*. 1997;43:754–760.
9. Pipus G, Plazl I, Koloini T. Esterification of benzoic acid in microwave tubular flow reactor. *Chem Eng J*. 2000;76:239–245.
10. Hoogenboom R, Wilms AFT, Schubert SU. Microwave irradiation—a closer look at heating efficiencies. *Aust J Chem*. 2009;62:236–243.
11. Chemat F, Poux M, Di-Martino JL, Berlan J. A new continuous-flow recycle microwave reactor for homogeneous and heterogeneous chemical reactions. *Chem Eng Technol*. 1996;19:420–424.
12. Patil NG, Hermans AIG, Benaskar F, Rebrov EV, Meuldijk J, Hulshof LA, Hessel V, Schouten JC. Energy efficient and controlled flow processing under microwave heating by using a milli reactor-heat exchanger. *AIChE J*. 2012;58:3144–3155.
13. Patil NG, Benaskar F, Rebrov EV, Meuldijk J, Hulshof LA, Hessel V, Schouten JC. Continuous multi-tubular milli-reactor with a Cu thin film for microwave assisted fine-chemical synthesis. *Ind Eng Chem Res*. 2012;51:14344–14354.
14. Comer E, Organ MG. A microreactor for microwave-assisted capillary (continuous flow) organic synthesis. *J Am Chem Soc*. 2005;127:8160–8167.
15. Comer E, Organ MG. A microcapillary system for simultaneous, parallel microwave-assisted synthesis. *Chem Eur J*. 2005;11:7223–7227.
16. Shore G, Yoo W, Li C, Organ MG. Propargyl amine synthesis catalysed by gold and copper thin films by using microwave-assisted continuous-flow organic synthesis (MACOS). *Chem Eur J*. 2010;16:126–133.
17. He P, Haswell SJ, Fletcher PDI. Microwave heating of heterogeneously catalysed Suzuki reactions in a micro reactor. *Lab Chip*. 2004;4:38–41.
18. He P, Haswell SJ, Fletcher PDI. Efficiency, monitoring and control of microwave heating within a continuous flow capillary reactor. *Sens Actuators B*. 2005;105:516–520.
19. Datta AK, Geedipalli SSR, Almeida MF. Microwave combination heating. *Food Technol*. 2005;59:36–46.
20. McMinn WAM, McLoughlin CM, Magee TRA. Thin-layer modeling of microwave, microwave-convective, and microwave-vacuum drying of pharmaceutical powders. *Drying Technol*. 2005;23:513–532.
21. Bonnet C, Estel L, Ledoux A, Mazari B, Louis A. Study of the thermal repartition in a microwave reactor: application to the nitrobenzene hydrogenation. *Chem Eng Process*. 2004;43:1435–1440.
22. Saillard R, Poux M, Berlan J, Audhuy-Peaudecerf M. Microwave heating of organic solvents: thermal effects and field modelling. *Tetrahedron*. 1995;51:4033–4042.
23. Robinson J, Kingman S, Irvine D, Licence P, Smith A, Dimitrakis G, Obermayer D, Kappe CO. Understanding microwave heating effects in single mode type cavities—theory and experiment. *Phys Chem Chem Phys*. 2010;12:4750–4758.
24. Sturm GSJ, Stefanidis GD, Van Gerven T, Verweij MD, Stankiewicz AI. Design principles of microwave applicators for small scale process equipment. *Chem Eng Process*. 2010;49:912–922.
25. Rakesh V, Seo Y, Datta AK, McCarthy KL, McCarthy MJ. Heat transfer during microwave combination heating: computational modeling and MRI experiments. *AIChE J*. 2010;56:2468–2478.
26. Rakesh V, Datta AK, Walton JH, McCarthy KL, McCarthy MJ. Microwave combination heating: coupled electromagnetics- multiphase porous media modeling and MRI experimentation. *AIChE J*. 2012;58:1262–1279.
27. Comsol A. B. "COMSOL Multiphysics Computational Fluid Dynamics module user's guide." version 4.2a, 2011.
28. Abe K, Kondoh T, Nagano Y. A new turbulence model for predicting fluid flow and heat transfer in separating and reattaching flows-I. *Flow field calculations. Int J Heat Mass Transfer*. 1994;37:139–151.
29. Ignat L, Pelletier D, Ilinca F. A universal formulation of two-equation models for adaptive computation of turbulent flows. *Comput Methods Appl Mech Eng*. 2000;189:1119–1139.

Manuscript received Feb. 21, 2014, and revision received June 3, 2014.